PLASMA HEATING BY ALFVEN WAVE IN FIELD-REVERSED ION RING EXPERIMENT

A Thesis

Presented to the Faculty of the Graduate School

of Cornell University

In Partial Fulfillment of the Requirements for the Degree of

Master of Science

by

Dongwoo Lee

Aug 2011

ABSTRACT

Controlled thermonuclear fusion is considered by many as a promising alternative energy source for the world's increasing energy demands. There are two main approaches towards thermonuclear fusion. One is called inertial confinement fusion and the other is called magnetic confinement fusion. Magnetic confinement fusion research can be categorized into two groups depending on the magnetic field topology. The Tokamak, which is a current mainstream plasma confinement device, is the toroidal device with a small poloidal field superimposed on a strong toroidal magnetic field so as to provide particle confinement and macroscopic stability. It is a very complicated machine in practice. Open field systems are generally soleniodal and often utilize magnetic mirrors to minimized end losses. An open mirror system can be given the advantages of the closed Tokamak system by introducing an axis-encircling current in the plasma that reverses the applied on-axis magnetic field and results in closed poloidal field lines. This configuration can, in principle, confine plasma as effectively as the Tokamak but without the complexity of Tokamak system. However, there are two major issues that have stood in the way of utilizing this configuration as a fusion reactor. First, no practical formation for a field reversed configuration at reactor scale size has yet been demonstrated. Second, the long standing contradiction between MHD predictions of instability and the observed stability of small experimental FRCs is still not fully understood.

The goal of the FIREX (Field-reversed Ion Ring Experiment) was to create a field-reversed configuration (FRC) in which a substantial fraction of the diamagnetic current was carried by energetic, axis-encircling ions, and to investigate the stability of this configuration. The FIREX program has established that strongly diamagnetic ion rings immersed in plasma, with ring ion velocities in excess of the Alfven speed in the

plasma, can be violently unstable to generation of compressional Alfven waves with wavelengths short compared to the ring orbit size. Two-dimension, axi-symmetric numerical simulations showed that the momentum transferred to the Alfven wave would take axial energy from the ring and cause the ring to come to a stop and be contained axially in the plasma. The FIREX experiment was designed to take advantage of this effect. However, in the experiment, the ring is not trapped. Magnetically insulated proton collector data showed that most of the protons exit through the ends of the solenoid within ~ 0.6μs of injection, or about 5 ion gyro-periods in the solenoid field. The reason for the rapid axial loss of the ring protons can be found in the magnetic field probe data. Intense high-frequency field fluctuations in the ring annulus were observed that do not propagate far radially. We believe that these very intense field fluctuations are waves generated by the collective interaction of the ring protons with the plasma. Their generation takes energy from the ring protons preferentially from their rotational motion. Numerical simulation results show rotational energy loss and similar, very strong Alfven turbulence generated within the ring annulus. The energy coupled from the ring to the waves is dissipated very locally in the plasma. The waves damp very rapidly in time after the ring ions are lost, and do not propagate far radially from their region of generation. The result must be very strong, local plasma heating, which has been seen in two ways in the experiment. The first is the observation of plasma diamagnetism. This diamagnetic field, with a characteristic decay time of ~2μs, can be seen clearly in the delta-B signal in the beam annulus. This smoothly decaying diamagnetism is seen only in and near the ring annulus, between 9 and 14cm radius. The second indication of heating is the direct measure of increased plasma ion kinetic energy by Doppler broadening of ion and neutral emission lines integrated across the plasma radius

BIOGRAPHICAL SKETCH

Dongwoo Lee, raised in Seoul, Rep. of Korea, graduated in 1995 from Seoul Science High School. During his high school years, he won medals in mathematical competitions, both domestic and international. He entered Seoul National University that spring as an electrical engineering major, with an emphasis in plasma physics. After graduating from Seoul National University, he started his first graduate study in Cornell University as an M. Eng student in electrical engineering, with Professor David A. Hammer as his advisor. After graduating in 2000 fall, he decided to continue his study as an M.S. student. His main research area was on high energy ion ring interaction with plasma.

ACKNOWLEDGMENTS

Foremost, I would like to express my gratitude towards my advisor, Professor David A. Hammer who has been of a great support. The same gratitude should be expressed to my committee members, Professor Bruce R. Kusse and Michael C. Kelley, for their support. John B. Greenly and Bill J. Podulka has been a continuous advisor during my graduate study, as they provided both academic and personal support. I also want to say thank you to Harry Wilhelm for his excellent job as a technician of the lab. Boris Knyazev and Alexei V. Gretchikha provided essential academic advices for my work and my thesis could not be complete without their assistance.

I am very thankful to the U.S. Department of Energy Office of Fusion Energy Sciences for granting research funding to this FIREX experiment, allowing me to perform experiment and research during my graduate school years.

TABLE OF CONTENTS

Chapter One

Field Reversed Configuration Approach To Magnetic Confinement Fusion

Controlled thermonuclear fusion is considered by many as a promising alternative energy source for the world's increasing energy demands. There are two main approaches towards thermonuclear fusion. One is called inertial confinement fusion, in which a laser beam, energetic particle beams or x-ray source is focused onto a small pellet containing a D-T (deuterium-tritium) mixture which is subsequently compressed and heated to thermonuclear conditions. The plasma created is confined only by its own inertia. The other approach is magnetic confinement fusion, in which a D-T mixture is heated by plasma internal currents and by auxiliary methods such as neutral or charged particle beams, electromagnetic waves, or magnetic compression, to thermonuclear conditions. The plasma in this situation is confined by magnetic fields.

Magnetic confinement fusion research can be categorized into two groups depending on the magnetic field topology. Closed systems are generally toroidal, with the advantage that there are no ends in the system and particle losses must occur across field lines. The Tokamak, which is a current mainstream plasma confinement device, is the toroidal device with a small poloidal field superimposed on a strong toroidal magnetic field so as to provide particle confinement and macroscopic stability. It is a very complicated machine in practice, especially when all necessary power reactor systems are included.

Open systems are generally solenoidal and often utilize magnetic mirrors to minimized end losses. In a conventional magnetic mirror, particles with sufficient velocity along the field lines are not reflected by the mirrors and can escape along the field line. An open mirror system can be given the advantages of the closed Tokamak system by introducing an axis-encircling current in the plasma that reverses the applied on-axis magnetic field and results in closed poloidal field lines. This configuration can, in principle, confine plasma as effectively as the Tokamak. There are, however, two major issues that have stood in the way of utilizing this configuration as a fusion reactor.

First, no practical formation method for a Field Reversed Configuration at reactor scale size has yet been demonstrated. This difficulty comes from the same property that makes an FRC so desirable as reactor plasma, i.e. the plasma and its self-field are not small perturbations on an imposed vacuum magnetic field, and there is no demonstrated way to smoothly and gradually build up the magnetic configuration from such a field.

Second, the long standing contradiction between MHD predictions of instability and the observed stability of small experimental FRCs is still not fully understood, allowing very little confidence in scaling of stability to larger plasmas. It has been thought that kinetic or large-orbit effects of ions in experimental FRCs contribute to their robust global stability.

The field-reversed configuration (FRC) was first predicted to be magnetohydrodynamically (MHD) unstable to an n=1, m=1 perturbation (“tilt instability”) by Rosenbluth and Bussac [1], and shortly thereafter it was

suggested that energetic ion beams could be employed to stabilize the mode[2]. Subsequent linear MHD analysis [3,4,5,6] confirmed the original predictions of instability but, in spite of theoretical predictions, experiments advanced to routinely produce FRC's with lifetimes of 30-50 MHD growth times. The attempts to resolve this discrepancy have focused on nonlinear and nonideal MHD effects[7,8], and kinetic effects[9,10,11]. Inclusion of nonlinear and nonideal MHD effects did not lead to substantial reductions in the predicted growth rate for normal experimental conditions. Kinetic studies, however, showed a substantial reduction in growth rate for s<3. The parameter s is a measure of the number of ion gyroradii separating the magnetic null from the separatrix, defined as

$$s = \int_R^{r_s} \frac{rdr}{r_s \rho_i}, \qquad (1)$$

where R is the radius of the magnetic null, r_s is the separatrix radius, and ρ_i is the local ion gyroradius. There is now some evidence[12] that tiltlike MHD activity may make formation difficult for s substantially greater than about 3. In any case, it is now generally believed that kinetic effects play a major role in the stabilization of the n=1 tilt mode for plasmas with s<3, and that some other external stabilizing influence, such as ion beam injection, may be required to increase s substantially beyond this value. In one recent simulation work[13], Barnes and Milroy demonstrated that ion beam injection provides an optimal way of adding the required kinetic effects to maintain a stable FRC.

On the other hand, the major result of our ion ring program has been to identify destructive smaller-scale instabilities that can be strongly driven by ring-like distributions of energetic ions. Numerical simulations by Alexei

Gretchika[14] also predicted that in energetic ion ring-plasma systems based upon magnetic cusp injection, like FIREX, collective interaction of the ring current with compressional Alfven waves in the plasma indeed generates extremely large-amplitude (>0.1T, with an applied B of 0.7T) magnetic fluctuations and rapid ring energy loss. Thus, the stability properties of such ring-like plasma systems are in question.

The goal of the FIREX (Field-reversed Ion Ring Experiment) was to create a field-reversed configuration (FRC) in which a substantial fraction of the diamagnetic current was carried by energetic, axis-encircling ions, and to investigate the stability of this configuration. Current research indicates that energetic neutral beam injection is the strongest candidate for the source of current and heat to build the FRC to the required flux and temperature, as well as possibly being required for angular momentum control to avoid spin-up of the plasma by ion-electron drag. As these injected neutrals strip in the FRC, a population of energetic, axis-encircling ions would be built up in the FRC as it is raised to the desired conditions. Thus, the end result would be exactly the configuration of our program goal. Also, as it is shown that large-orbit ions can contribute both to large-scale stability and to small-scale instability[13], it is more important than ever to understand the physics of the ring-FRC system without having to wait for a reactor-scale plasma to be made.

The FIREX program has established that strongly diamagnetic ion rings immersed in plasma, with ring ion velocities in excess of the Alfven speed in the plasma, can be violently unstable to generation of compressional Alfven waves with wavelengths short compared to the ring orbit size. FIREX can

produce rings of axis-encircling 0.5MeV protons with 100kA of diamagnetic current over 5cm. The rings are created by using a pulsed-power generator (0.7MV, 0.5MA and 120ns pulse length) to generate an annular proton beam in a magnetically-insulated ion diode. The beam is injected axially across a magnetic cusp into the solenoid. The flux crossed in the cusp produces axis-encircling ring orbits, with more than 80% of the ion energy in rotation. The residual axial velocity moves the ring along the 2m length of the solenoid. The rings are confined to a ~0.1m radius in a 0.6T field initially containing a $10^{20}m^{-3}$, ~5eV hydrogen plasma. The plasma diamagnetism is initially negligible. The ion ring current by itself is not enough to reverse the field, but it does reduce the field on axis by up to 0.2T. This excluded flux increases the field outside the ring but within the cylindrical aluminum vacuum vessel wall by 0.1T. These are the most strongly diamagnetic ion rings yet attained.[14,15] This substantial fraction of field reversal enables study of the dynamics of ion ring plasma interaction in a regime relevant to what is desired in an FRC. The outstanding feature of the interaction of these rings with the background plasma is the generation of very large amplitude (~0.2T) Alfven waves, which have profound effects upon both the ring and the plasma.

The rotational velocity of the hydrogen ions (~1 * 10^7 m/s) is above the Alfven speed of ~5 * 10^5 m/s in the background plasma; the Alfven Mach number is 20. The axial ring velocity is about 10^6 m/s, which is comparable to Alfven speed. Thus the ~0.1μs injection time of the ring occurs in a time shorter than the ~0.5μs radial Alfven transit time in the 0.25m radius vessel. The result is that the entering ring's diamagnetic field is instantaneously shielded by currents induced in the background plasma, and then the field

appears and propagates radially away from the ring as a compressional Alfven wave.

Two-dimension, axi-symmetric numerical simulations[14] showed that the momentum transferred to the Alfven wave would take axial energy from the ring and cause the ring to come to a stop and be contained axially in the plasma. The FIREX experiment was designed to take advantage of this effect. However, in the experiment, the ring is not trapped. Magnetically insulated proton collector data showed that most of the protons exit through the ends of the solenoid within ~ 0.6μs of injection, or about 5 ion gyro-periods in the solenoid field.

The reason for the rapid axial loss of the ring protons can be found in the magnetic field probe data. Intense high-frequency field fluctuations in the ring annulus were observed that do not propagate far radially. We believe that these very intense field fluctuations are waves generated by the collective interaction of the ring protons with the plasma. Their generation takes energy from the ring protons preferentially from their rotational motion. Numerical simulation results show rotational energy loss and similar, very strong Alfven turbulence generated within the ring annulus.

The energy coupled from the ring to the waves is dissipated very locally in the plasma. The waves damp very rapidly in time after the ring ions are lost, and do not propagate far radially from their region of generation. The result must be very strong, local plasma heating, which has been seen in two ways in the experiment. The first is the observation of plasma diamagnetism. This

diamagnetic field, with a characteristic decay time of ~2μs, can be seen clearly in the delta-B signal in the beam annulus. This smoothly decaying diamagnetism is seen only in and near the ring annulus, between 9 and 14cm radius. The second indication of heating is the direct measure of increased plasma ion kinetic energy by Doppler broadening of ion and neutral emission lines integrated across the plasma radius. There are the principal results that constitute this master's thesis. They are presented in detail in Chapter 3, after the FIREX experiment is described in Chapter 2.

Chapter TWO

Experimental Setup

Section A: FIREX facility

Figure **1** shows the configuration of Cornell's field-reversed ion ring experiment, FIREX. A pulse-forming line driven by a 300kJ Marx generator delivers ~600kV and ~600kA peak voltage and current to the ion diode, producing 100kA of protons. The FIREX diode, shown in detail in

Figure **2**, has a 7mm gap and ~1MV/meter electric field, which causes the plastic anode to break down electrically and form plasma. (This field is about 10 times more than is required to generate plasma.) Ions produced from the anode are turned into an ion ring by passing through the radial magnetic field region between the anode and cathode. The electrons produced from the cathode are magnetically insulated, the electron current being reduced by factor of 40 compared to without any magnetic field. This diode has carefully designed field line shape, with several flux conservers in place, to accomplish this high level of magnetic insulation. The flux conservers experience 10~20 tons of force when the magnetic field coil in the anode is pulsed, and so substantial support structure that is not shown in Fig. 2 is required.

FIREX also includes two Z-discharge plasma electrodes that are approximately 1 meter apart in the region downstream of the ion diode. The upstream electrode is located just downstream of the cusp region. The downstream electrode is a multi-pin electrode with a flashboard pre-ionizer to improve the promptness and uniformity of the discharge. Ring propagation into

low-density gas fills that have been pre-ionized is significantly better than for low-density fills that are not pre-ionized, and ring propagation in a nominally uniform plasma is better than in a very non-uniform plasma.

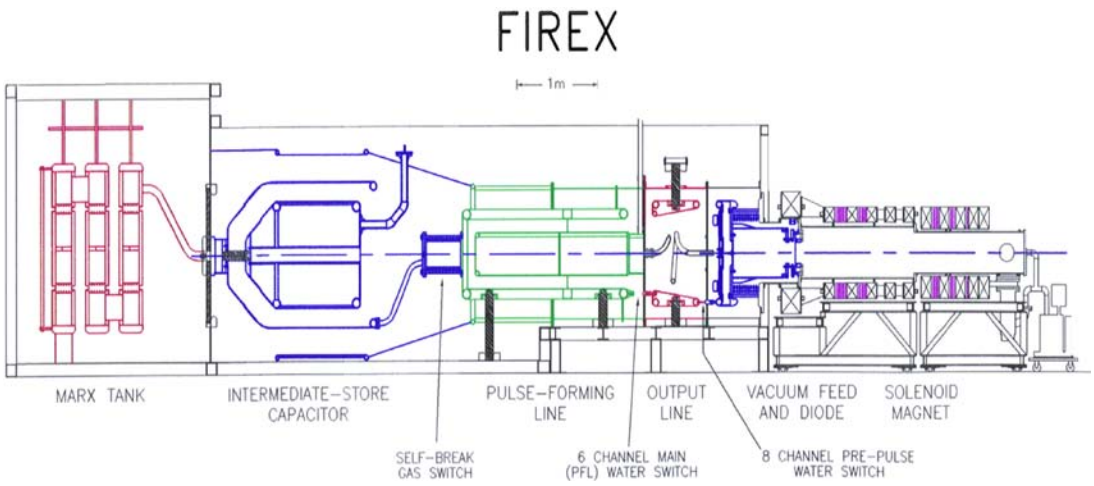

Figure 1 FIREX Facility Diagram

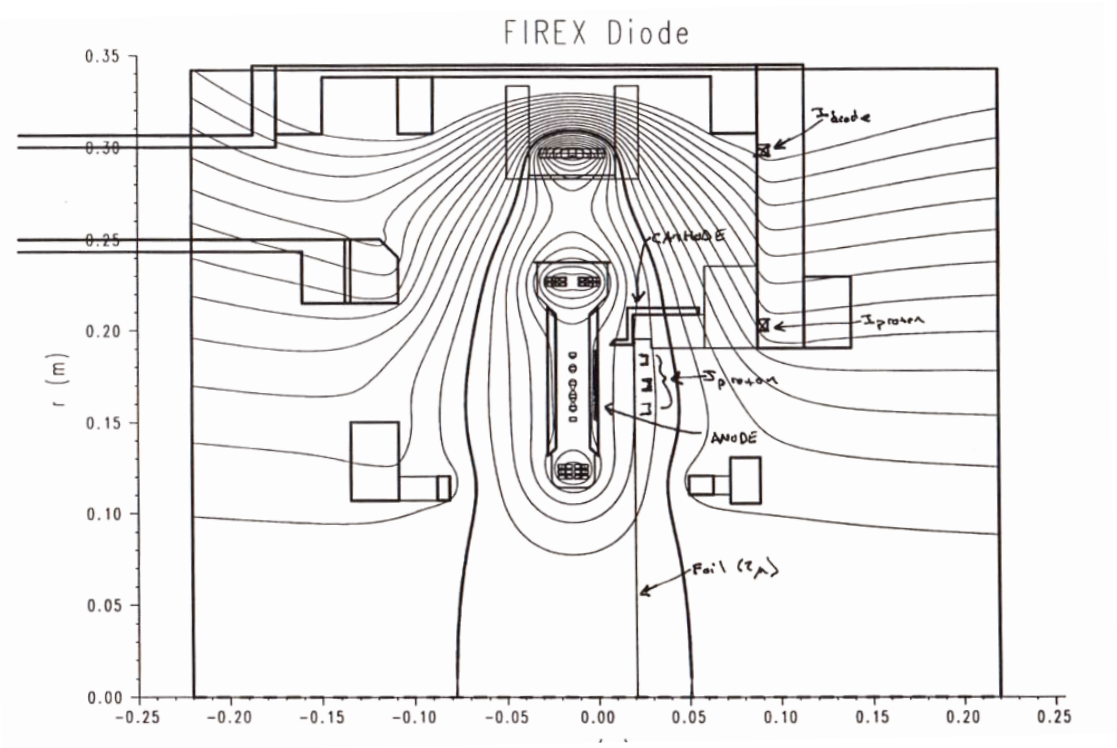

Figure 2 FIREX Diode Diagram with Magnetic Field Lines

Section B: Optical diagnostics

A combined system of a spectrometer and a streak camera was used to obtain visible light spectra as a function of time. The light from the plasma was collected in an optical fiber through a quartz window on the side of the experiment chamber. The quartz window is located 18cm from the diode, which is only a few centimeters away from the upstream plasma discharge electrode. To ensure that light or cold particles from the discharge electrode don't interfere with the measurement by being close to or in the field of view, we chose the location of field of view to be at 40cm from the diode. A set of mirrors were installed to transfer the light from the field of view to the window, forming a periscope without any housing. A convex lens was used to enhance the efficiency of light collection.

Figure **3** and

Figure **4** show the setup in the chamber to deliver the light to the optical fiber.

The other end of the fiber is placed in front of the entrance slit of the monochromator, with another convex lens in place between the fiber and the input slit, for the same reason as above. The VM521 1-m grating monochromator from Acton Research Cooperation disperses the light input in wavelength space with a wavelength resolution of 0.014nm with a 10um input slit. The light output was focused into the input slit of a streak camera by three lenses, including one achromatic cylindrical lens. The output light of this C2830 streak camera from Hamamatsu (with M2548 slow speed streak sweep unit) was amplified by two micro-channel plates and was recorded on the film in a Nikon FE2 camera. This system was originally designed and installed to use a CCD camera instead of a film camera by Boris Knyazev, but due to

damage of the CCD camera and lack of money and time to repair it, we decided to use a film camera that was available in the lab. The output optics system was adjusted to be compatible with a film camera. The film was developed in the lab and scanned with a Minolta Dimage film scanner using Minolta scan software.

Figure **5**,

Figure **6** and

Figure **7** show these later stages of the optical analysis setup.

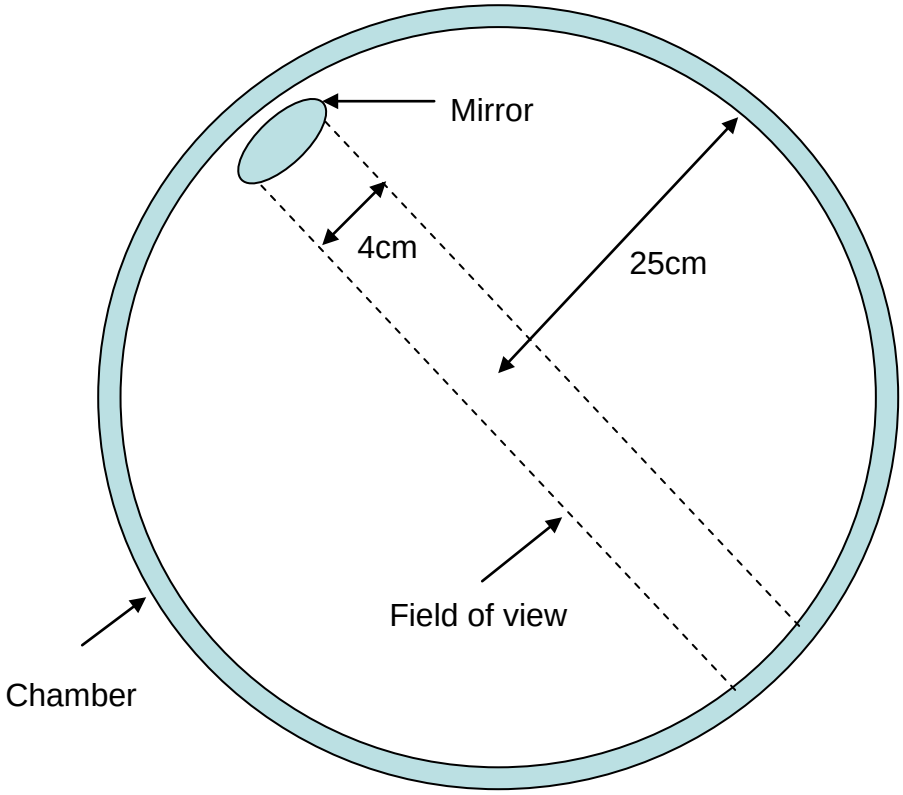

Figure 3 r-theta cross-section at 40cm from the diode

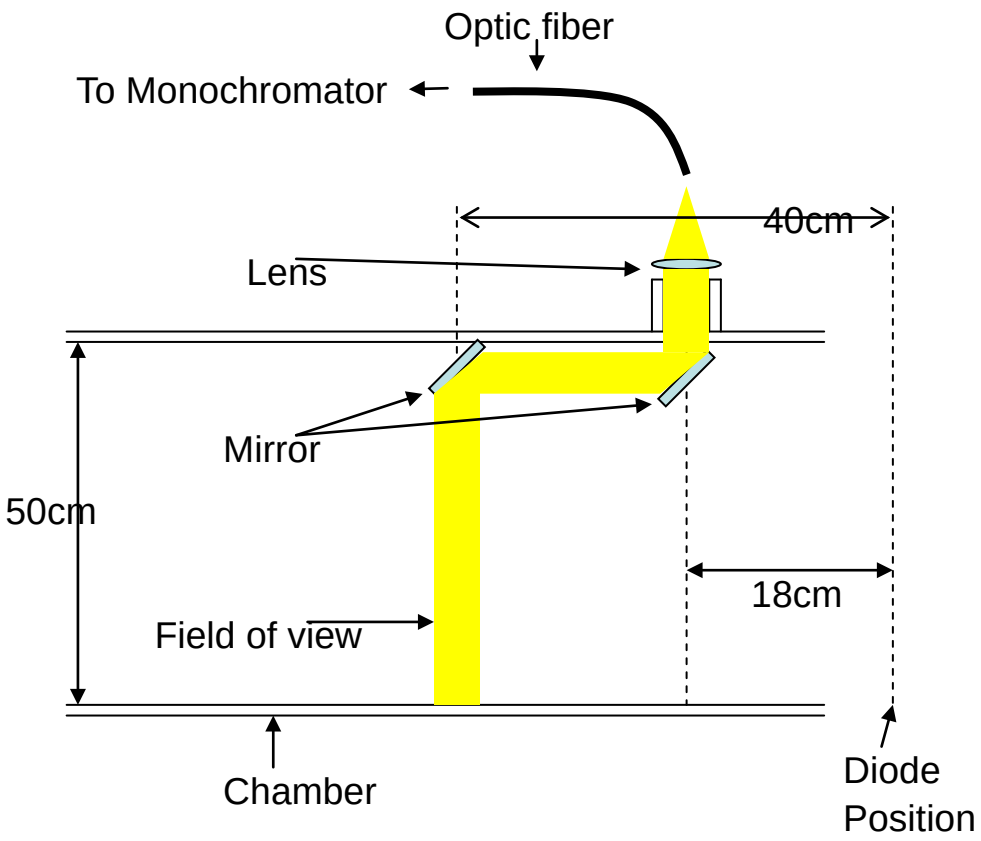

Figure 4 r-z cross-section of optical setup in the chamber

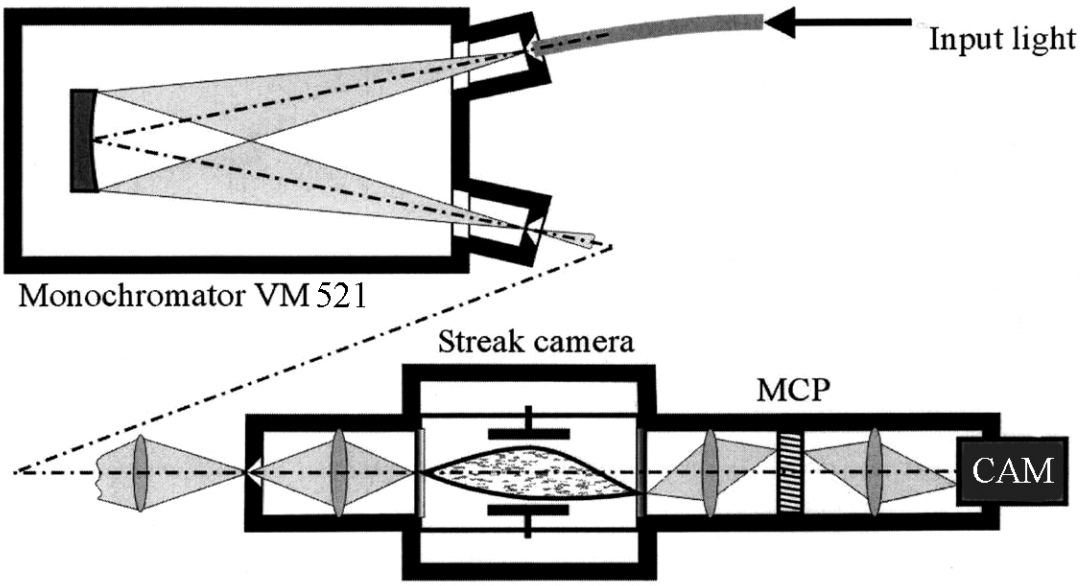

Figure 5 Optical System Setup Diagram

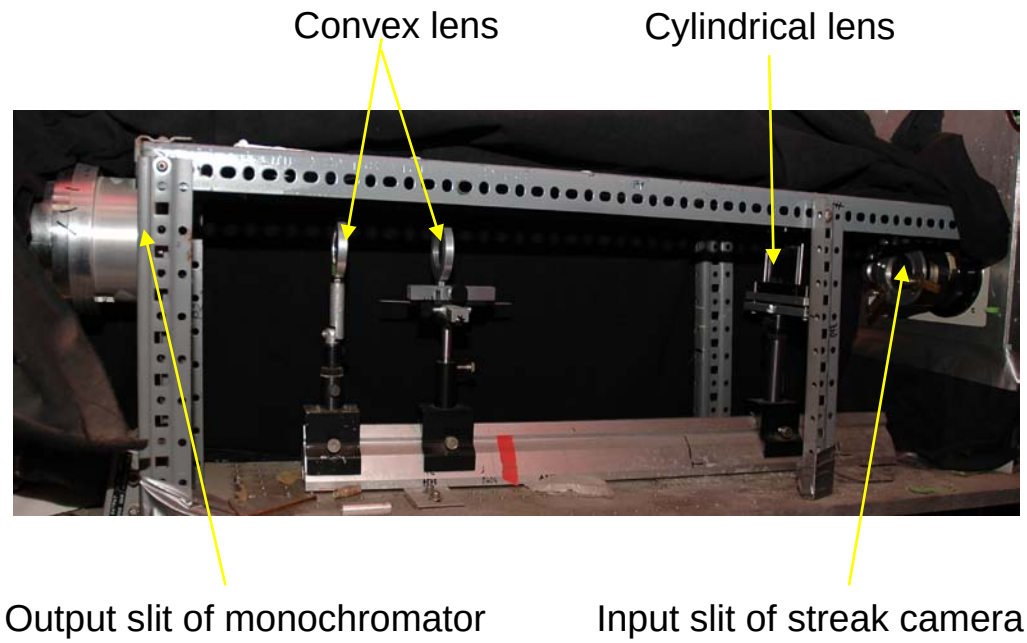

Figure 6 Picture of Optical System Setup

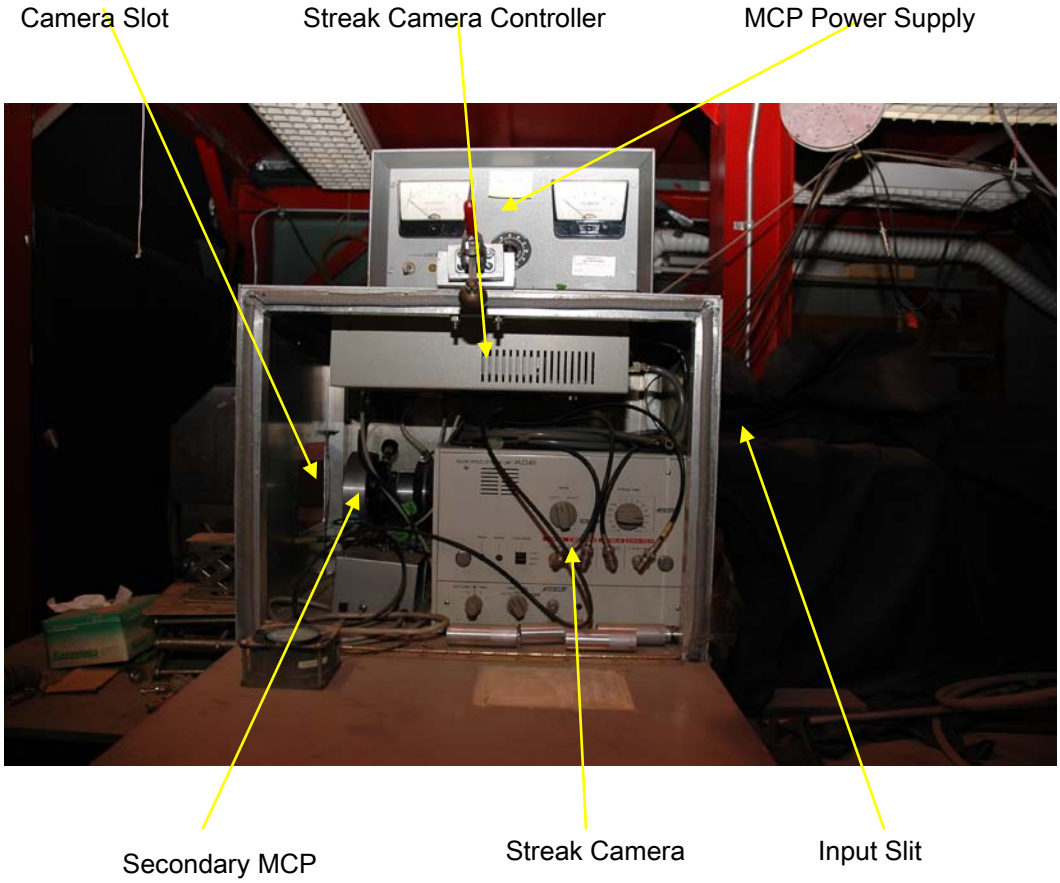

Figure 7 Streak Camera Setup

Section C: Magnetic probe

A magnetic probe, or B-dot probe, is a small coil that can measure the change of the B field in the direction of the axis of the coil. The basic principle of the magnetic probe is that a time varying field induces a current in a conducting coil. From Faraday's law of electromagnetic induction, i.e. $\bar{\nabla} \times \bar{E} = -\frac{\partial \bar{B}}{\partial t}$, and surface integral on both sides and use Stoke's theorem on left-hand side yields, $\oint_C \bar{E} \cdot d\bar{l} = -\int_S \frac{\partial \bar{B}}{\partial t} \cdot d\bar{s}$ and since the circuit is stationary during the shot, the time derivative can be moved outside of the surface integral so $\oint_C \bar{E} \cdot d\bar{l} = -\frac{d}{dt}\int_S \partial \bar{B} \cdot d\bar{s} \approx -\frac{d}{dt} B \cdot A$, where A is the coil area.

So the output voltage from the coil is proportional to the cross sectional area of one turn times the number of turns in the coil and times the time-derivative of the magnetic field. The magnetic probe output is integrated electronically by a passive RC integrator and the integrated signal represents the magnetic field values. The probe used here was first designed by William J. Podulka[16], and it was maintained with some modifications for this research.

Chapter THREE

Ring-Plasma Interaction

As briefly discussed in Chapter I, the energy coupled from the ring to the waves is dissipated very locally in the background plasma. Therefore, strong local heating in the background plasma should be observable. The first observation method is spectroscopy, which directly measures the plasma ion temperature and/or the directed ion kinetic energy from the Doppler broadening and/or shift of emission lines.

Section A: Calibrations prior to actual data acquisition

To ensure the accuracy and reliability of this spectroscopy system, the following calibrations were done before acquiring and analyzing spectra from FIREX. The first step was to establish the correct wavelength calibration so that we could correlate the spectral lines on film with precise wavelengths. A He-Ne laser with a wavelength of 6328.3Å was used as the first step of this wavelength calibration. Using a laser light source has advantages over using normal spectral lamps. First, there is only one wavelength in the laser light while each spectral lamp has spectral lines with various wavelengths. Therefore we could eliminate the possibility of making an error in determining the wavelength of the observed spectral line. Second, laser light does not disperse much over distance, so we can visually confirm that the light is properly positioned and focused at any given point along the optical path by placing a screen or a piece of white paper in the beam path. Then with spectral lamps, we checked the accuracy of the wavelength scale of the monochromator. The focusing should be adjusted at each wavelength since

we used only one achromatic lens in the optical system. Coarse adjustment was done by moving the lenses while looking at the viewfinder of the camera, and then several pictures of the light from each spectral lamp were taken with slightly different lens positions. The final optimal focusing condition was selected by comparing those pictures.

The second step was to establish the correct time scale calibration of the streak camera. The system trigger signal was applied to a PT-55 pulse generator from Pacific Atlantic Electronics, and the arcing light at the gap between the output and ground of the PT-55 was observed using the optical system. The current signal confirmed that the light exists only for less than 1μs, so we could obtain a reasonably accurate time scale calibration.

The final step was to obtain absolute light intensity information from the developed film. This can be done by applying the response curve of the film. However, the developing conditions may vary from one pulse to the next, and the condition of the developer chemicals may change this curve and produce significant error in the light intensity information. To help eliminating this variable, an unexposed picture and a fully exposed (saturated) picture were taken with the spectrogram picture. This provides the information about the developing condition, which can be used as a correction factor for the response curve and a response curve corrected by using this information was used to minimize the error caused by changes in chemicals used during development of film.

Section B: Interpretation of acquired line profile

The scanned data was analyzed using Mathcad software from MathSoft. This routine reads the scanned film data as an input, fits a Gaussian curve to the line at given time and determines the width of the line. The light intensity calibration is done after reading the data in, as described above. The temperature of the plasma ions at that time can be calculated using a Doppler broadening model, assuming the velocity distribution is Maxwellian, and assuming all other non-instrumental broadening mechanisms are negligible.

The corrections for instrumental widths of the streak camera and the monochromator are included in this calculation.

If $\delta\lambda$ is the measured width of a line, the corrected width, $\delta\lambda G$ is[17],

$$\delta\lambda G = \sqrt{(\delta\lambda)^2 - {\lambda_{res}}^2 - {\delta\lambda_{sc}}^2} \tag{2}$$

where λ_{res} is the spectral resolution of the monochromator with the slit width we have used and $\delta\lambda_{sc}$ is the streak camera instrumental width.

In the Doppler broadening model, the observed frequency f is,

$$f = f_0\left(1 \pm \frac{\upsilon}{c}\right) \tag{3}$$

where f_0 is the frequency for an atom at rest, υ is the speed of the emitter in the direction of observation and c is the speed of light.

Assuming a Boltzmann distribution of speeds, the distribution of radiation around the center frequency is then,

$$I(f) = I_0 \exp\left[\frac{-m_0 c^2 \left(f - f_0\right)^2}{2kT{f_0}^2}\right] \tag{4}$$

This is a form of Gaussian, and the full width at half maximum is

$$\Delta f_{Doppler} = \frac{2 f_0}{c}\sqrt{2\ln 2 \frac{kT}{m_0}} \quad \text{or} \quad \frac{\Delta\lambda}{\lambda_0} = \frac{2}{c}\sqrt{2\ln 2 \frac{kT}{m_0}} \tag{5}$$

So by equating the calculated value of $\delta\lambda G$ to $\Delta\lambda$, we can, in principle, obtain the temperature of the plasma at a given time.

The fitting of a Gaussian curve to the spectral line profile obtained experimentally is not always straightforward. In many cases, the line does not have a Gaussian curve shape, so the accuracy or effectiveness of fitting should be considered before we discuss temperature data. There are several instrumental errors that can change the line shape, as well as some 'real' physical reasons. First we have to find the reason why some line shapes are not Gaussian. The possible instrumental errors are saturation of the micro-channel plate (MCP), saturation of the film and scintillation of the phosphor screen. The saturation of MCPs or film can be confirmed by comparing pictures with similar levels of light input. If we have a flat-top line shape in one picture and if there are other points in the same picture that show Gaussian line shapes with stronger light intensity, then we can confirm that the flat top profile is not caused by saturation. With this method, we confirmed that the saturation problem is not an issue with our optical measurement in most cases. The scintillation issue can be addressed by examining a picture taken with constant illumination delivered to the streak camera input. Test pictures were taken with ambient room light. As can be seen in Figure 8, there are repetitive peaks, roughly ~1 Å apart. This pattern contributes to the line shape distortion you can see in Figure 9.

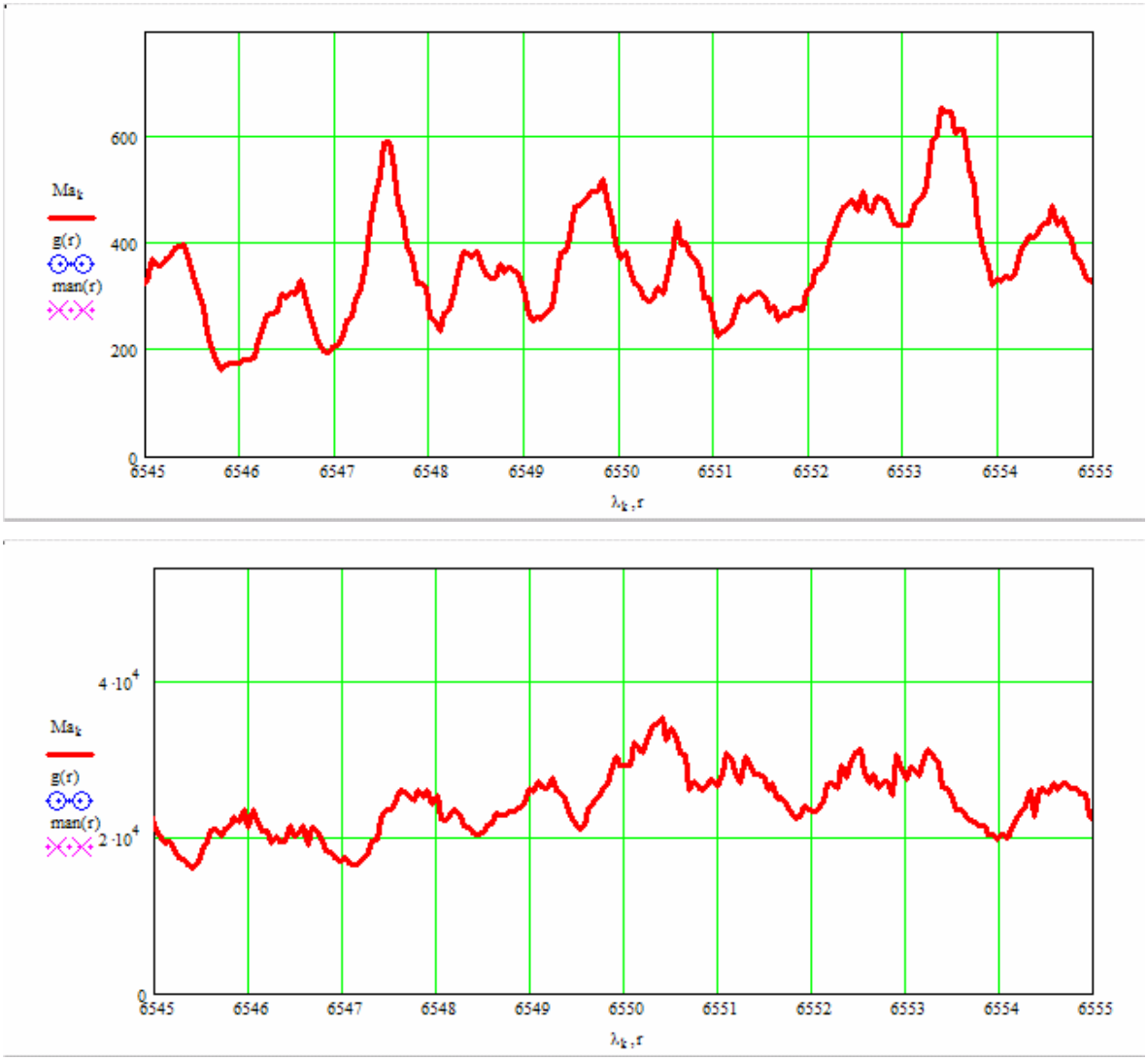

Figure 8 Ambient room light pictures taken in focus mode, with different light intensity. The wavelength scale reflects relative distance on the screen, not actual wavelength.

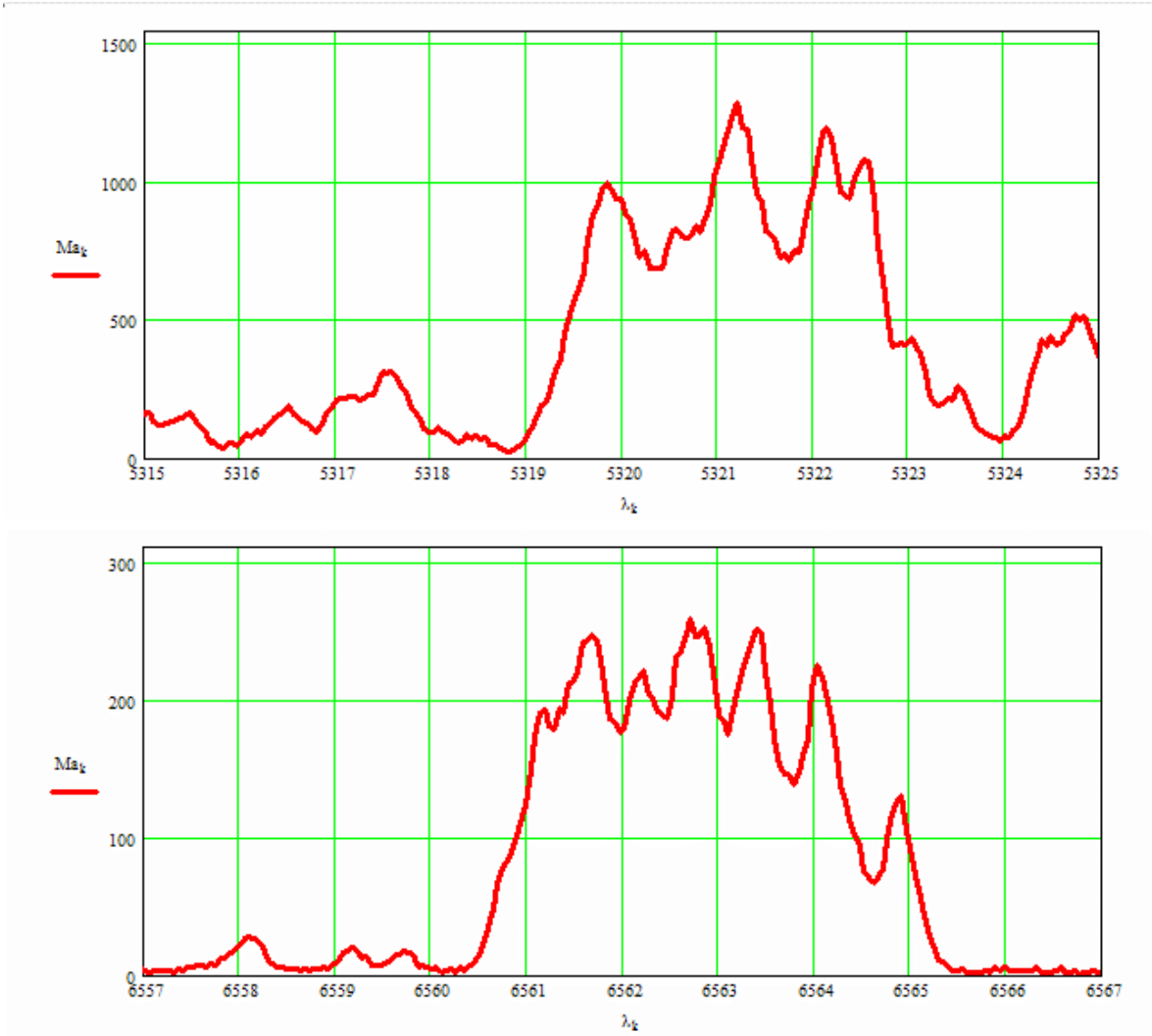

Figure 9 Examples of non-Gaussian line shapes: Doubly ionized Nitrogen line (top), and the Hydrogen-alpha line. Wavelength (x axis) is in units of Angstrom, and the light intensity (y axis) is in arbitrary units.

Section C: Results from the Optical Diagnostic System

In FIREX, the background gas used to generate plasma was mainly hydrogen so it was reasonable to search for a hydrogen spectral line as the first step. A spectral line at 6562.8Å, which is the H-alpha line, was the first choice since this line has the strongest relative intensity in the Balmer series. In a thermal equilibrium state, about 2eV of temperature is sufficient to fully ionize hydrogen gas so the line will disappear if the temperature exceeds this temperature. However, in FIREX the heating process has a very short time scale, and so because of the relatively slow ionization rate, thermodynamic equilibrium is not achieved and the plasma is not fully ionized. Therefore, it is possible for the H-alpha line to be observed even if the electrons have a higher temperature than 2eV. In addition, the ion temperature can be higher than the electron temperature so it is possible for the H-alpha line to be observed even when the hydrogen ions have higher energy than the ionization energy.

Typical results from a Hydrogen fill shot are shown in the series of figures, from 10 through 13.

A picture of the film with streak image of shot 600 is shown in

Figure **10**. The scanned image of this film is shown in

Figure **11**. Each band in the scanned image represents the area that is averaged to produce one line profile. The evolution of the line profile is shown in Figure 12, with the fitted Gaussian curve for each line profile. Each line profile is obtained from successive bands in

Figure **11**. Those typical results from hydrogen fill shots are chosen from 25

good data shots.

The indicated temperature of the hydrogen plasma based on the Doppler width of the spectral lines reaches 15~20eV at 10~15μs after the ring is injected into the plasma. After this first peak, the light intensity decreases for 5~10μs and temperature decreases with the light intensity. After this period of low light, low temperature interval, both the light intensity and temperature climb back up and the temperature reaches ~15eV at 30~35μs after ring injection.

This H-alpha line data represents the temperature of the neutral atoms, not ions. Ion temperature information is more useful to understand the plasma. A singly ionized Nitrogen line was found at 5679.56Å. The same Doppler broadening model is used to calculate the temperature of Nitrogen ions. The most obvious difference between this N-II line data and H-alpha line data is the indicated temperature of N-II line is much higher than that obtained from the H-alpha line data. Typical results are shown in Figure 14. The temperature based on the Doppler width reaches ~200eV or more, at ~10μs after the beam injection. The duration of the high temperature peak is 2~3μs, which is similar to the H-alpha line. The light intensity at the high temperature peak is higher than that of H-alpha line, but the light intensity decreases faster and the light is weaker than that of H-alpha line later on, i.e. ≥ 30μs after ring injection. The temperature of the N-II ions also decreases below 100eV. Those typical N-II line data are chosen from 16 good data shots.

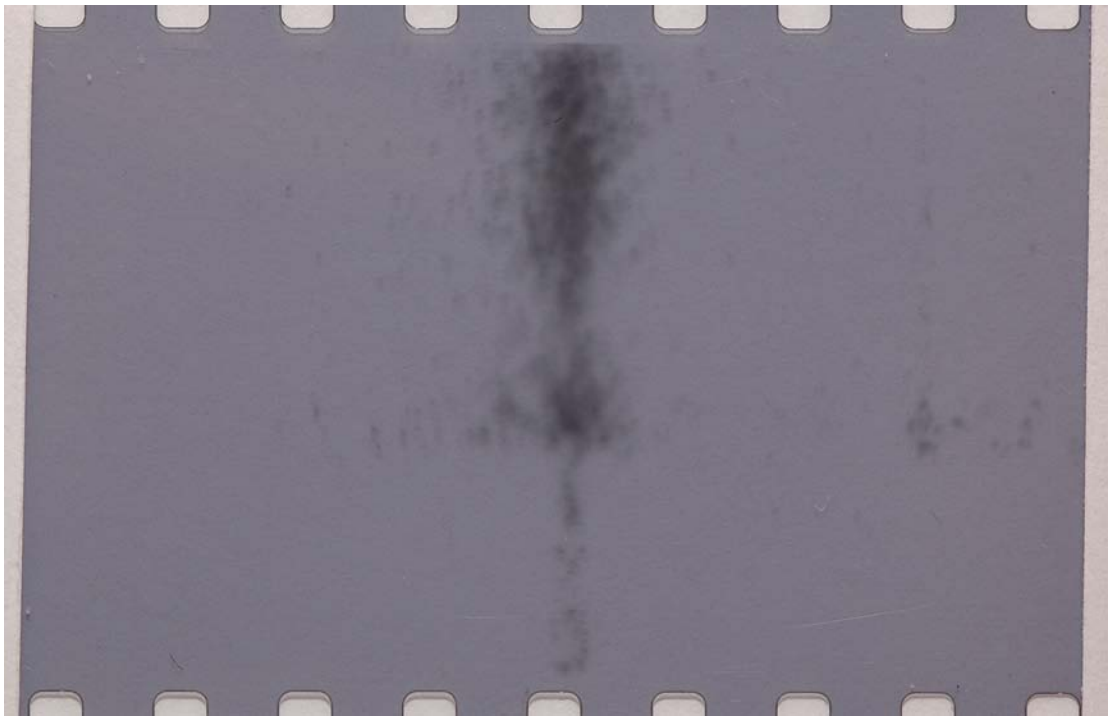

Figure 10 Picture of the film from shot 600

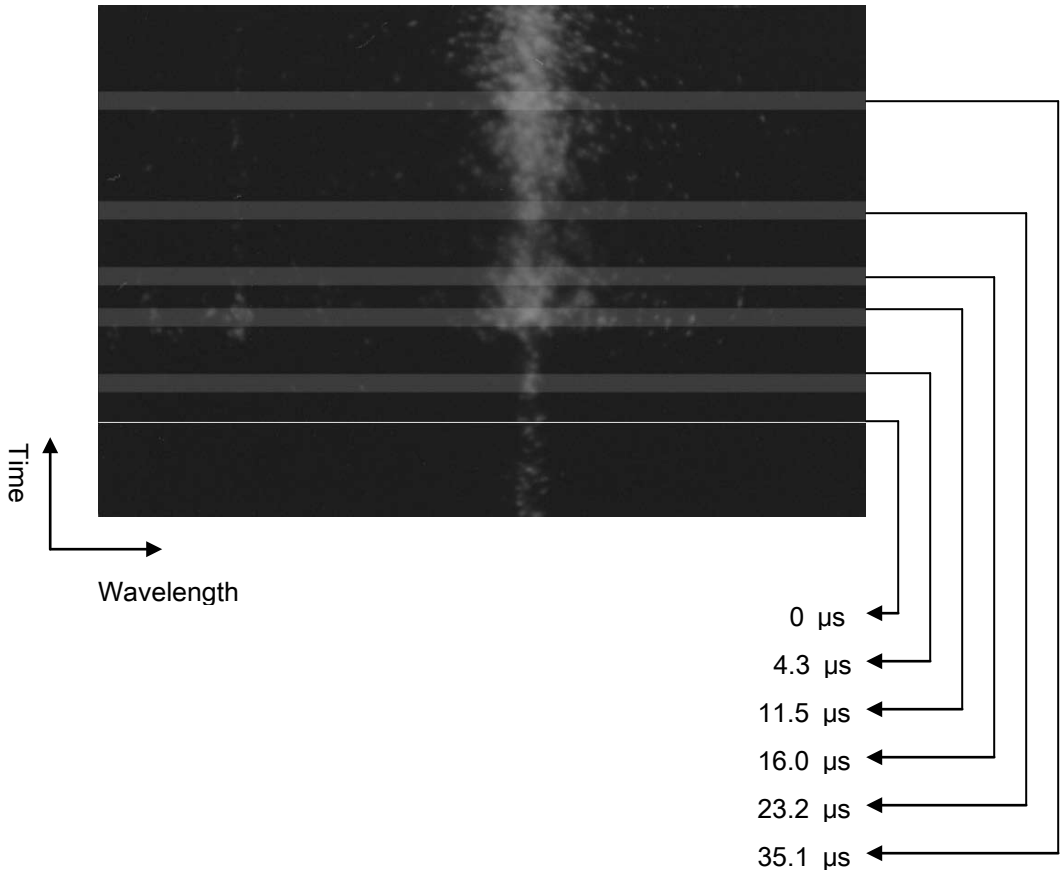

Figure 11 Scanned image from shot 600 (Scanned image of Figure 10)

Five bands represent area of film averaged to produce a line profile for respective time points

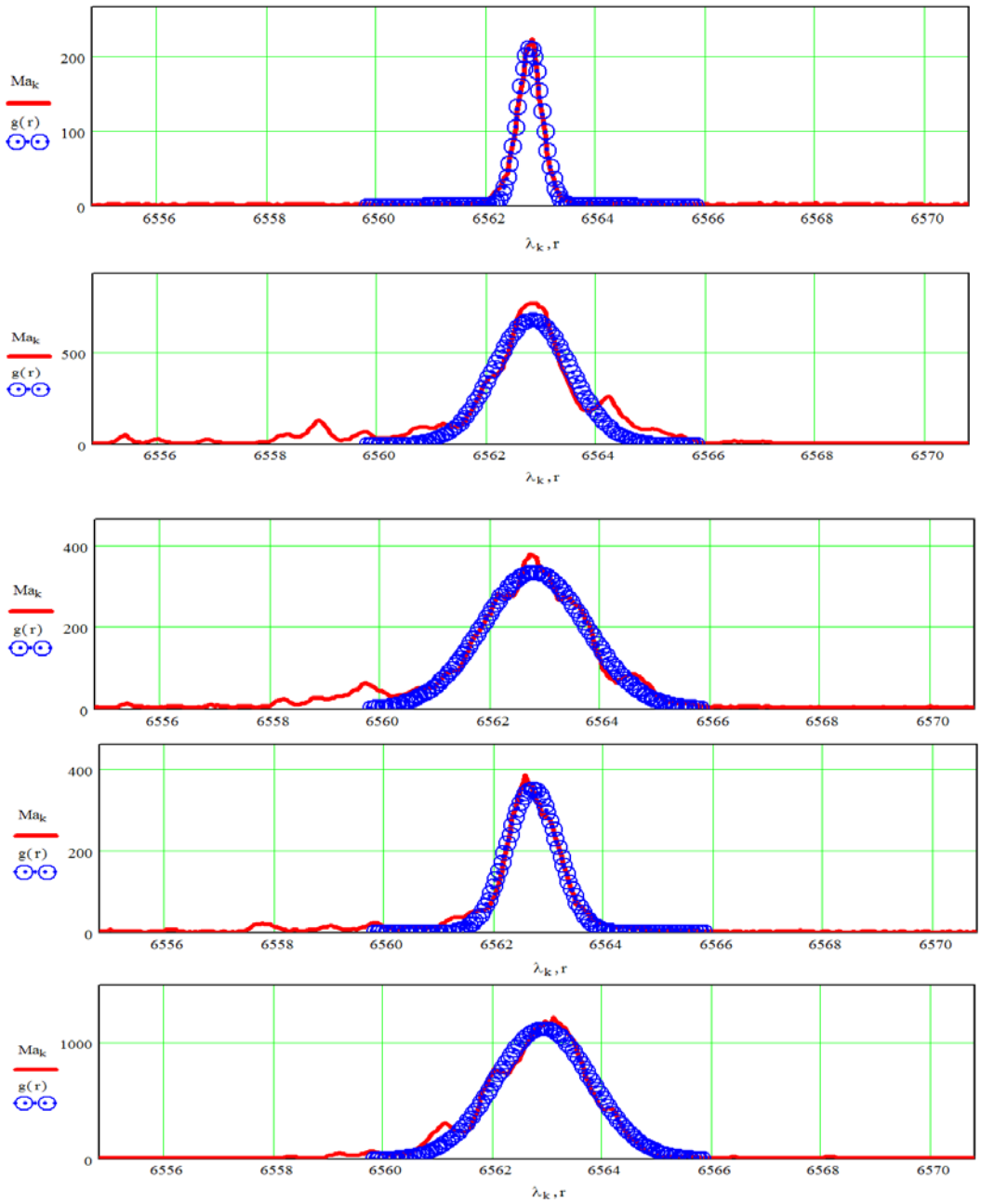

Figure 12 Evolution of the H-alpha line profile, from shot 600, at t=4.3μs, 11.5μs, 16.0μs, 23.2μs and 35.1μs

Wavelength (x axis) is in Angstroms and light intensity (y axis) is in arbitrary units.

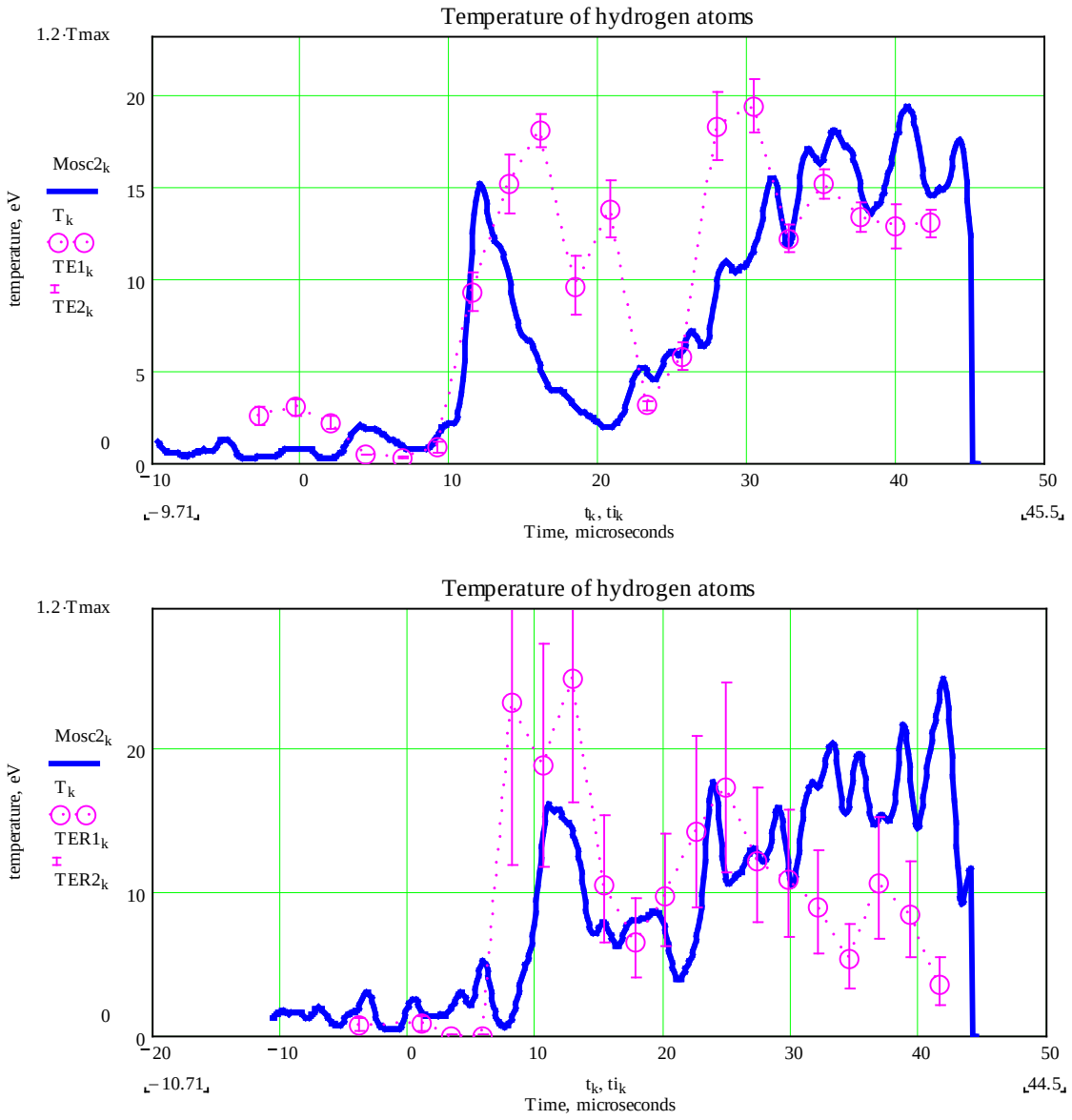

Figure 13 Shot 600 (top) and Shot 601 (bottom), with 4mTorr of Hydrogen fill. The solid line (labeled as Mosc2k) represents the light intensity and the dotted line (labeled as Tk) represents the temperature of the Hydrogen atoms. The scale for light intensity is arbitrary

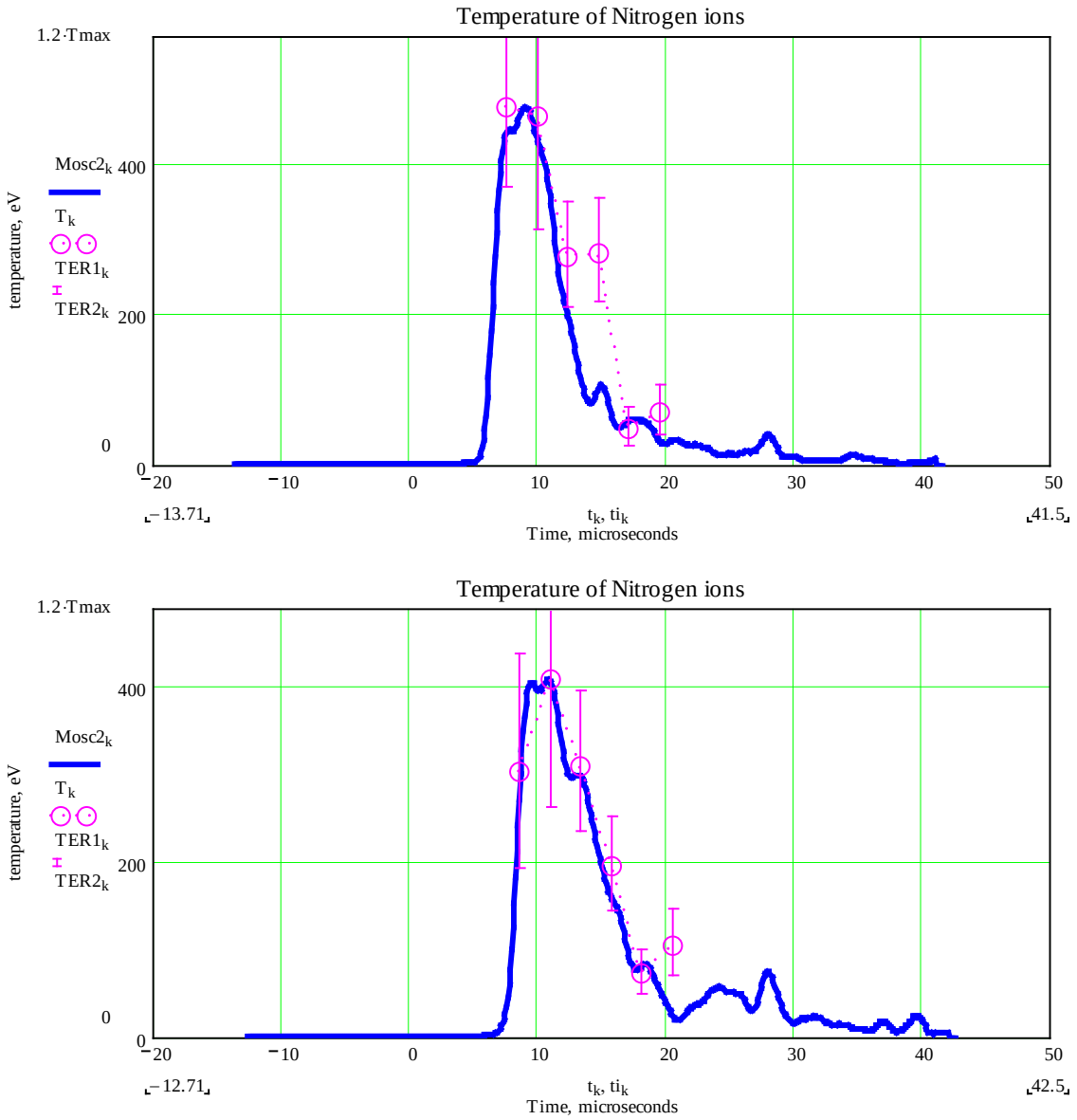

Figure 14 Shot 640 (top) and shot 641 (bottom), with 3mTorr of Nitrogen fill. The solid line (labeled as Mosc2k) represents the light intensity and the dotted line (labeled as Tk) represents the temperature of the singly ionized Nitrogen ions. The scale for light intensity is arbitrary.

To increase the credibility of ion temperature data, another line with higher charge state was observed. A doubly ionized Nitrogen line was found, at 5320.82Å. Figure 15 shows a typical result for the ion temperature inferred from the width of this line. The peak ion temperature is over 500eV, even higher than the inferred peak temperature from singly ionized Nitrogen. The light usually increases a lot slower than the singly ionized Nitrogen line intensity, but the maximum intensity reaches a similar level to the maximum of the singly ionized line intensity later in time. The light intensity of the doubly ionized line increases almost monotonically after 20μs, and reaches its maximum value around 40μs. As shown in the figures, the temperature also roughly follows the light intensity, increasing temperature from 20μs until 40μs, reaching up to 500~600eV. Those typical N-III line shots are chosen from 12 good data shots.

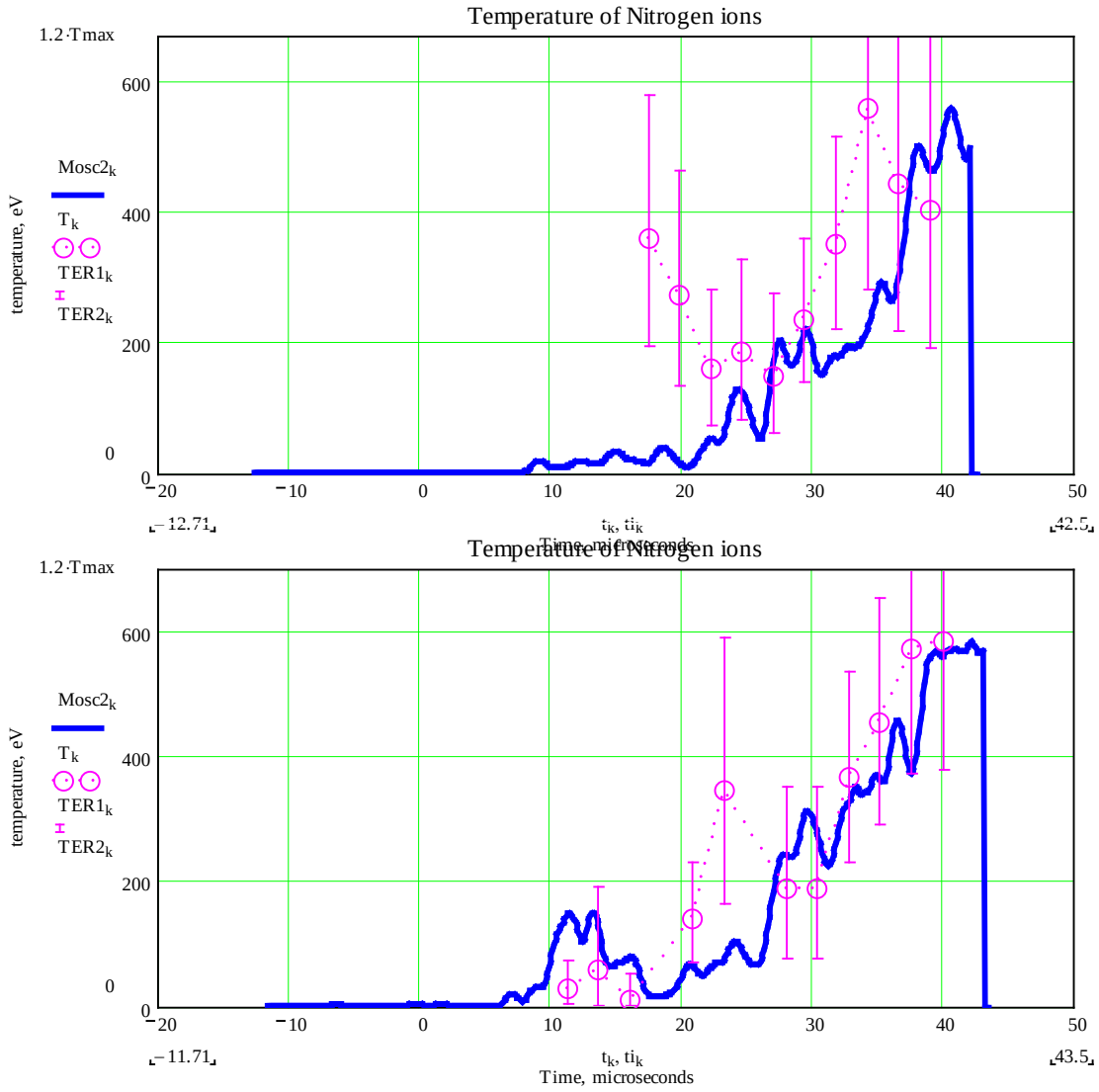

Figure 15 Shot 642 (top) and shot 643 (bottom), with 3mTorr of Nitrogen and 1mTorr Hydrogen fill, respectively. The solid line (labeled as Mosc2k) represents the light intensity and the dotted line (labeled as Tk) represents the temperature of doubly ionized Nitrogen ions. The scale for light intensity is arbitrary.

Section D: Comparison of optical diagnostic data and other diagnostic data

The spectral measurement of the plasma ion temperature measures the temperature of the plasma that is in the line of sight of the optical system, while the B dot loop measures the change of the magnetic field at the specific location where it is placed. These two measurement systems are located only a few centimeters apart from each other. Therefore, comparing those two sets of data can help understand the plasma.

Figure 16 shows the typical passively integrated B dot probe signals from a hydrogen background fill shot. By comparing these data with the spectroscopy data, the most obvious difference is the time scale difference. In the spectroscopy data, the ion temperature rises 7~10μs after the beam injection, but in B dot probe signal, the diamagnetism starts 1~2μs after the beam injection. The diamagnetism from the ring itself is very big so it is difficult to determine the exact starting time of the diamagnetism due to plasma temperature, but it clearly starts a lot earlier than the spectroscopy. By the time the spectroscopy data shows the rise of the ion temperature, the diamagnetism is almost gone and less than 10% of the diamagnetism remains.

The other difference between those two data is the temperature. The spectroscopy temperature shows that it rises up to ~20eV around 10μs after the beam injection. The diamagnetism caused by this temperature should be given by

$\sum nkT + \frac{B^2}{2\mu_o} = const.$, which becomes $\Delta B \approx \frac{\mu_0}{B} \cdot \sum nk\Delta T$ (6)

The density n can be calculated from the period of the Alfven waves, i.e., the oscillation period in Figures 16 and 17,

$$v_A = \frac{B}{\sqrt{\mu_o \rho}} = \frac{B}{\sqrt{\mu_o M_i n}}, \tag{7}$$

with $B = 0.7T$ and $v_A = 5 \times 10^5 m/s$. Therefore the density $n \approx 9 \times 10^{20} m^{-3}$.

By plugging these numbers into equation (6), the diamagnetism ΔB should be about 0.005T, (or 50G) which is more than factor of 10 smaller than the peak field obtained with the B dot probes. At 10μs after the beam injection, the B dot probe data shows comparable amount of diamagnetism, but the sensitivity of the B dot probe at this scale of diamagnetism at this late time is not reliable because of the noise correction process. Therefore it is not really possible to say that the spectroscopy data and the B dot probe data agree at later time.

Figure 17 shows a typical passively integrated B dot probe signal from the nitrogen background fill shot. Unlike the hydrogen shot case, there is no significant time delay between the damping of the wave and the start of the heating in the spectroscopic results.

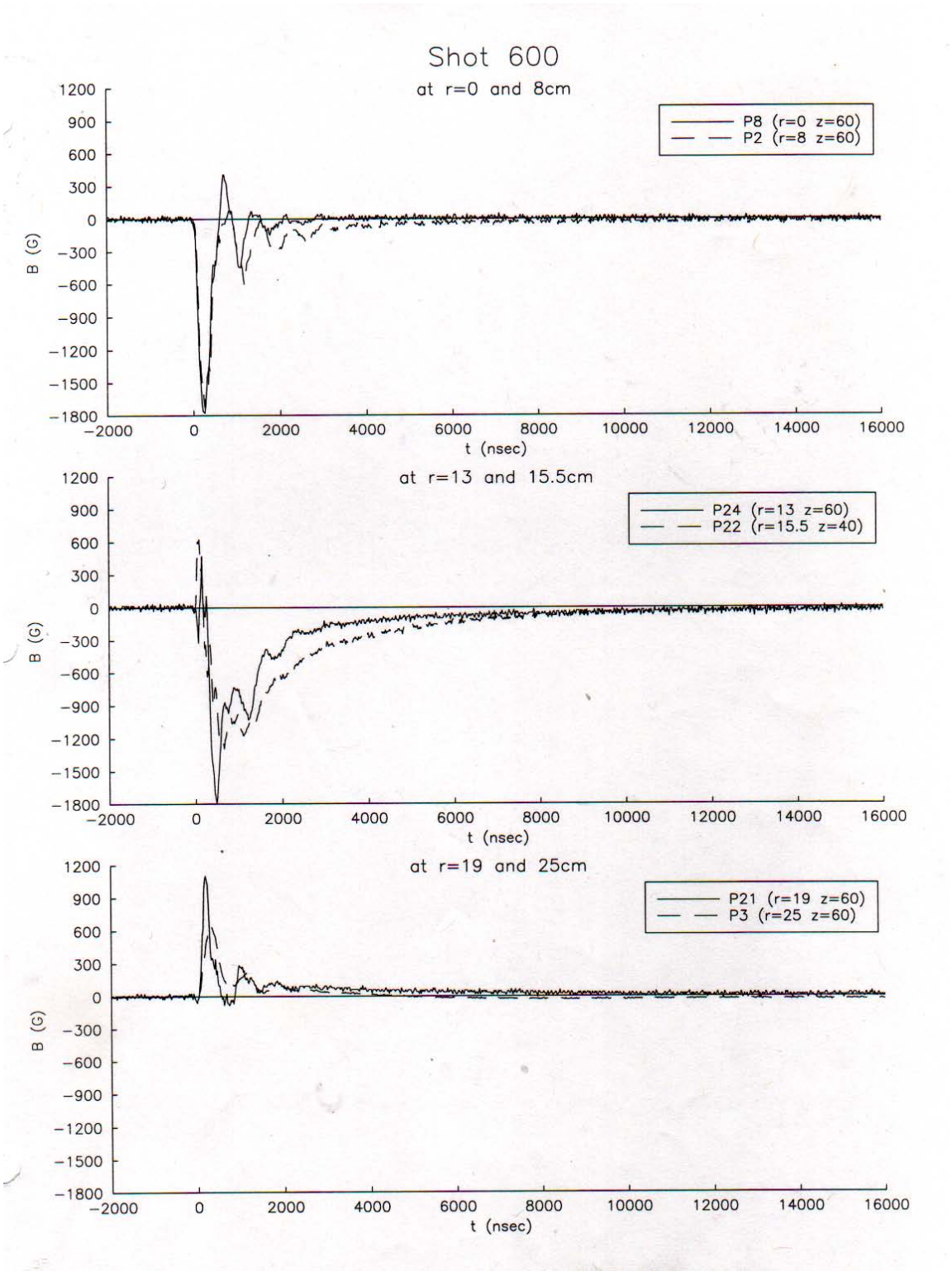

Figure 16 Magnetic field from Shot 600 (hydrogen fill) at 6 different radii.

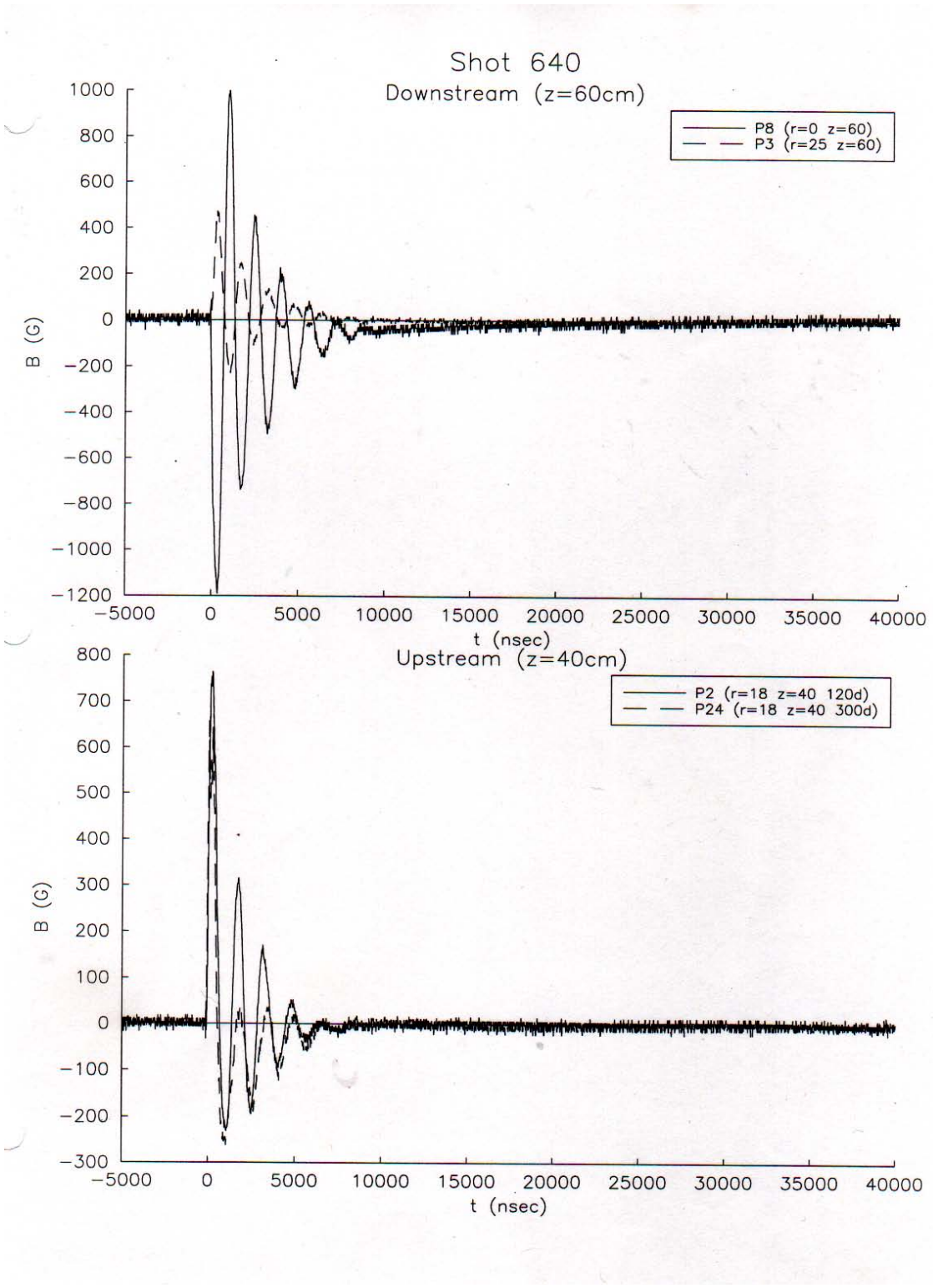

Figure 17 Magnetic field from Shot 640 (nitrogen fill) at 4 different radii

Now, let us calculate the inferred temperature from the magnetic field data. The first 500~700ns in the B dot probe data is the beam diamagnetism, and the Alfven wave is observed in the B dot probe. The wave is damped away very quickly so after 2~2.5μs, the wave is down to negligible size. The diamagnetism that appears in the beam channel after the wave is damped away can be considered as the diamagnetism in the background plasma. The P22 probe, which was at r=15.5cm, z=40cm, shows the strongest diamagnetism, around -700G (or -0.07T, 10% of applied B) at 2μs. Equation (6) can be used to calculate the ion temperature, and it give about 300eV, which is more than 10 times higher than the peak temperature in the spectroscopy data, and more than 100 times higher than the ion temperature from the spectroscopy data at 2μs.

We also notice that the total flux in the chamber is not conserved, by comparing B dot probe data from different radial locations. The ring channel (P24 and P22) shows strong diamagnetism but outside the channel probes do not show strong paramagnetism. However, in reality the total flux should be conserved, so we can conclude that the diamagnetism that we saw in the ring channel is a local phenomenon that occurs only near the probes. An interesting pair of B dot data sets are shown in Figure 18. Shot 589 and 593 were taken with the same settings except for the position of the B dot probe P21. The radial position of the P21 was at r=19cm for both shots, which is just outside of the ring channel. The azimuthal position is the variable in this set: in shot 589, P21 is located close (~4cm) to ring channel probe P22, while in shot 593 P21 is located far away (>15cm) from any other probes. Since P21 is outside of the ring channel, it should show a paramagnetic signal when the beam passes and then some wave activity after that time. This was true in

shot 593. However, in shot 589, P21 shows a diamagnetic signal starting at ~6μs after the beam injection. This is the evidence that the local activity around the probe may be caused by hot particles generated by ring ion bombardment of the probe and its structure. This was confirmed with other shots with magnetic probes located close together.

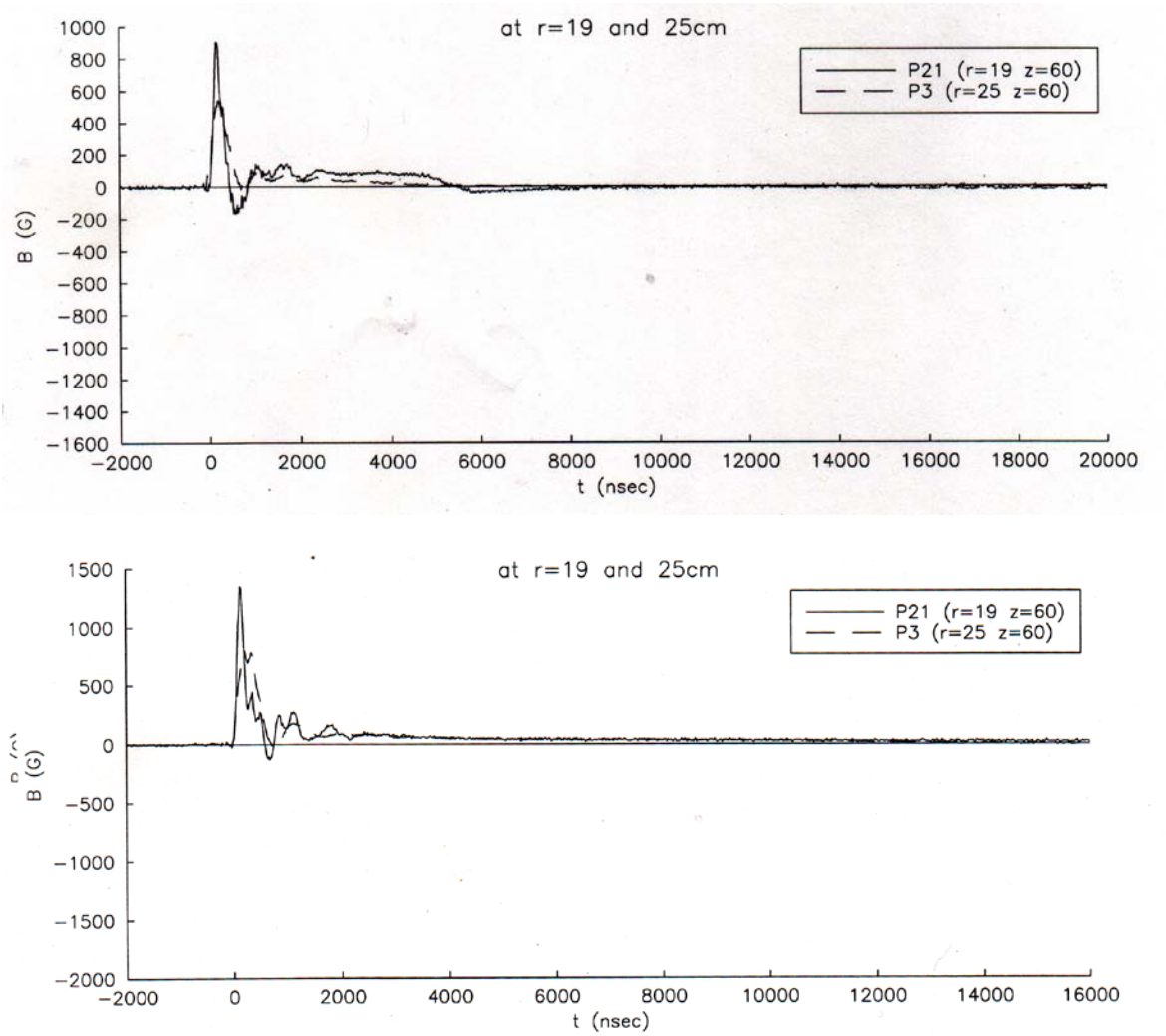

Figure 18 Magnetic Field from Shot 589 (top) and 593 (bottom)

This hypothesis can also explain the time difference and the temperature difference between the spectroscopy and the B dot probe data. If the diamagnetism is caused by hot particles around the probe caused by ion bombardment, then it means that the density of the plasma around the probe is higher than the background plasma, and the inferred temperature from the diamagnetic signal is lower than what we calculated above. Also, as those particles disperse, the density is going to decrease and that will reduce the diamagnetism, so this can explain why the diamagnetic signal on the B dot probes dies away even before the spectroscopy shows the start of the heating in the background plasma. The heating shown in the spectroscopy would imply only several tens of Gauss of diamagnetic signal on the probes, as we calculated above, so the major characteristic signals in the B dot probes do not relate to the spectroscopically observed heating of the background plasma. The integrated B dot probe signals usually have noise pickup from other electric signals, and despite of various efforts to minimize those noise pickups it was impossible to completely eliminate the noise pickup, so a noise correction was always required to obtain meaningful data from the raw probe signal. However, that correction process lowers the sensitivity and the reliability for the data at later time, so even if the B dot probe had detected the background heating, it is very likely that we could not recognize it after the correction process.

Section E: Discussion for the spectroscopy data

In section C, typical spectroscopy data were presented for hydrogen and nitrogen lines. Both the hydrogen alpha line and the single-ionized nitrogen line shows heating starting from about 10μs after beam injection. But for the hydrogen line, the background fill was hydrogen gas, and the Alfven wave from the magnetic probes (in section D) decays and damps down to negligible size in around 2μs. Therefore, there is some time delay between the decay of the wave and the start of the heating in spectroscopy. By contrast, for the nitrogen line the background fill was nitrogen gas and the damping rate of the wave is slower and there is no significant time gap. The speed of the 1eV hydrogen atom is approximately 10^6cm/s, so a 20eV atom will have a speed of about $4.6*10^6$cm/s. Therefore, the delay is comparable to the time that this atom travels the distance from the diode to the field of view, which is about 40cm. To check this hypothesis, we have to check the collision time of hot (about 20eV) hydrogen atoms traveling through cold (about 5eV or less) hydrogen atoms.

The slowing down or energy loss relaxation rate of hot hydrogen atoms can be calculated by using the following formulas:[18]

Slowing down: $$\frac{d\vec{v}_\alpha}{dt} = -\nu_s^{\alpha\backslash\beta} \cdot \vec{v}_\alpha \qquad (8)$$

Energy loss: $$\frac{d}{dt} v_\alpha^2 = -\nu_\varepsilon^{\alpha\backslash\beta} \cdot v_\alpha^2 \qquad (9)$$

Rates are associated with relaxation processes arising from the interaction of test particles (labeled α) streaming with velocity $\vec{v}_\alpha$ through a background of field particles (labeled β). The formulas for the relaxation rates can be written

$$\nu_s^{\alpha\backslash\beta} = (1+\frac{m_\alpha}{m_\beta})\psi(x^{\alpha\backslash\beta})\nu_0^{\alpha\backslash\beta}; \quad (10)$$

$$\nu_\varepsilon^{\alpha\backslash\beta} = 2\left[(\frac{m_\alpha}{m_\beta})\psi(x^{\alpha\backslash\beta}) - \frac{d}{dx}\psi(x^{\alpha\backslash\beta})\right]\nu_0^{\alpha\backslash\beta}; \quad (11)$$

where $\nu_0^{\alpha\backslash\beta} = 4\pi e_\alpha^2 e_\beta^2 \lambda_{\alpha\beta}\frac{n_\beta}{m_\alpha^2}\upsilon_\alpha^3$; $x^{\alpha\backslash\beta} = m_\beta\frac{\upsilon_\alpha^2}{2kT_\beta}$

$$\psi(x) = \frac{2}{\sqrt{\pi}}\int_0^x \sqrt{t}e^{-t}dt;$$

$\lambda_{\alpha\beta}$ is the Coulomb logarithm, and e_α is the charge of species α.

So for the case of hot hydrogen atoms traveling through relatively cold hydrogen atoms, the relaxation rates are

$\nu_s^{\alpha\backslash\beta} = 1.093\times10^{10}(cm^3\sec^{-1})$, $\nu_\varepsilon^{\alpha\backslash\beta} = 1.066\times10^{10}(cm^3\sec^{-1})$

Consequently, the heating seen in the hydrogen alpha line cannot be from upstream or any other place far from the field of view because it will be cooled down too fast. For nitrogen ions, the same formulas can be applied to calculate the relaxation rates, and those are $\nu_s^{\alpha\backslash\beta} = 7.138\times10^6(cm^3\sec^{-1})$, $\nu_\varepsilon^{\alpha\backslash\beta} = 1.303\times10^7(cm^3\sec^{-1})$ for hydrogen background plasma, and $\nu_s^{\alpha\backslash\beta} = 1.306\times10^8(cm^3\sec^{-1})$, $\nu_\varepsilon^{\alpha\backslash\beta} = 1.306\times10^8(cm^3\sec^{-1})$, for nitrogen background plasma. These results confirm that the heating seen in the spectroscopy is a phenomenon that occurs in (or close to) the field of view.

Since we confirmed that the heating really occurs in or close to the field of view, the time delay between the decaying of the Alfven wave and the start of the heating seen in the spectroscopy should be explained. The fact that nitrogen ion temperature is 15 ~ 20 times higher than hydrogen temperature

means that all the ions are accelerated to the same velocity, tied to the magnetic field lines. However, the heating that we observe is from the spectroscopy, which means that the existence of the spectral line does not depend on ion temperature but on electron temperature. The ion-electron thermal equilibrium time is,

$$\frac{dT_\alpha}{dt} = \sum_\beta \overline{\nu}_\varepsilon^{\alpha\backslash\beta}(T_\beta - T_\alpha) \tag{12}$$

where

$$\overline{\nu}_\varepsilon^{\alpha\backslash\beta} = 1.8\times10^{-19}\frac{(m_\alpha m_\beta)^{1/2} Z_\alpha{}^2 Z_\beta{}^2 n_\beta \lambda_{\alpha\beta}}{(m_\alpha T_\beta + m_\beta T_\alpha)^{3/2}} \tag{13}$$

Z is ion charge state, and $\lambda_{\alpha\beta}$ is the Coulomb logarithm.

For the hydrogen fill shot, assuming 20eV hydrogen ion temperature and $9\times10^{14}(/cm^3)$ electron density the thermal equilibrium time is $1.306\times10^{-7}(\sec)$. Consequently, we can conclude that the electron temperature will be high enough to make the light emission once the ions are heated, and the time delay between decaying of the Alfven wave and start of the heating in the spectroscopy means that the species which makes the light emission does not exist during that time period.

For the hydrogen alpha line shots with hydrogen background fill, hydrogen atoms will not be accelerated by the Alfven wave because the neutral atoms are not affected by the magnetic field change. Charge transfer collisions in which the fast ions collide with the slow neutral atoms, change the fast ions to fast neutrals. The charge transfer collision frequency ν is $n\overline{\sigma\upsilon}$, and it is $4.452\times10^5(\sec^{-1})$ for 20eV hydrogen, using the charge transfer cross section

of $8\times10^{-16}(cm^2)$ for hydrogen ion to hydrogen atom collisions[19]. So with the comparable charge transfer collision time, the delay in hydrogen fill shot is explained well. For the nitrogen ion line measurements with nitrogen background fill, there is no delay between the decay of the Alfven wave and start of the heating in the spectroscopy which also agrees with the previous explanation because it is an ion spectral line.

There are couple more questions to be answered, and one of them is the temperature difference between hydrogen and nitrogen ions. The temperature of nitrogen ions is much higher than hydrogen ions, and it stays at higher temperature for 5 to 10μs. The thermal equilibration time should be calculated to confirm that it is physically possible that those two species can exist together with more than factor 10 difference in terms of temperature for this time scale.

Thermal equilibration when two species have different temperatures but no relative drift is described by

$$\frac{dT_\alpha}{dt}=\bar{\nu}_\varepsilon^{\alpha\backslash\beta}(T_\beta-T_\alpha) \tag{14}$$

where $\bar{\nu}_\varepsilon^{\alpha\backslash\beta}=1.8\times10^{-19}\dfrac{(m_\alpha m_\beta)^{1/2}Z_\alpha^2Z_\beta^2n_\beta\lambda_{\alpha\beta}}{(m_\alpha T_\beta+m_\beta T_\alpha)^{3/2}}$ (15)

Z is ion charge state, $\lambda_{\alpha\beta}$ is the Coulomb logarithm.

For 400eV nitrogen ions with 20eV hydrogen ions, the thermal equilibrium time is about 60μs, which is longer than the current timescale. However, this calculation cannot be directly compared to our result, because first of all, all the shots with nitrogen line pictures were taken with nitrogen background fill. Therefore, there is no evidence that the hydrogen ions have the same

temperature as shots when the background was hydrogen. There still would be some amount of hydrogen in the chamber even for the shots with nitrogen background fill, but the densities of the hydrogen atoms and ions are not known.

The other question is the ion-electron thermal equilibrium time in nitrogen fill shots. Using equation (15), the ion-electron thermal equilibrium time can be calculated. For nitrogen fill shots, assuming 400eV of nitrogen ion temperature and $9\times10^{14}(/cm^3)$ electron density the thermal equilibrium time is $1.833\times10^{-6}(\text{sec})$. In previous calculations the ion-electron thermal equilibrium time in hydrogen fill shots is $1.306\times10^{-7}(\text{sec})$. Therefore, combining these two numbers means nitrogen ions and hydrogen ions will reach thermal equilibrium faster than we discussed in previous paragraph. Even though the ion-ion thermal equilibrium time is long enough to explain the temperature difference as we discussed above, those two ion species will reach thermal equilibrium through ion – electron – ion energy transfer. However, this does not directly contradict the experimental results, because all the hydrogen ion temperature data were acquired from hydrogen fill shots so the hydrogen ion temperature in nitrogen fill or hydrogen-nitrogen mixed fill is not known. Therefore, the hydrogen ion temperature could be as high as the nitrogen ion temperature a couple of microseconds after the plasma heating. Furthermore, the density of hydrogen in nitrogen fill shot is unknown so the ion-electron thermal equilibrium time for hydrogen ions is not very reliable.

Chapter FOUR

Conclusion

In previous chapters, we confirmed that the background plasma is heated by the energy coupled from the ring to the waves which was then dissipated in the plasma. The waves damp away significantly in only a few periods or less after the ring leaves and as a result, strong local plasma heating is observed. In hydrogen fill shots the temperature of hydrogen plasma reaches 15~20eV, and in nitrogen fill shots the temperature of nitrogen plasma reaches ~200eV or more. The energy relaxation calculation confirmed that this heating is a local phenomenon, and estimates of the charge transfer collision frequency calculation confirmed that this increase of ion temperature occurs at the right time compared to the decay of the Alfven wave. Furthermore, the fact that nitrogen ions are heated to a temperature 15~20 times higher than the temperature of hydrogen also confirms that the heating is done by waves because the temperature ratio of nitrogen to hydrogen is comparable to the mass ratio of nitrogen to hydrogen, which means the ions are accelerated to the same velocity.

There is still some more work to be done to complete the picture of plasma heating in FIREX. First of all, the difference of the temperature in nitrogen and hydrogen at the start of the heating process can be well explained but the fact that the difference seems to continue for extended time is still not fully understood. In particular, there is no data from nitrogen fill or nitrogen and hydrogen mixed fill tests with hydrogen spectral lines recording giving the actual temperature of hydrogen when there is nitrogen also present.

Also, the initial heating is done by the energy from the wave, which no

longer exists after the wave decay is finished. However, the temperature of ions continues to increase, particularly from doubly ionized nitrogen data, so the source of heating is not exactly known. The z-discharge plasma source is still operating at that time, so it is possible that the heating is done by the current from plasma source. Additional tests will be required to determine the source of late time heating in the plasma.

Reference

[1] M. N. Rosenbluth and M. N. Bussac, Nucl. Fusion 4,489 (1979).

[2] H. H. Fleishmann, in Proceedings of the US-Japan Joint Symposium on Compact Tori and Energetic Particle Injection (Princeton U. P., Princeton, NJ, 1979), p.41.

[3] A. I. Shestakov, D. D. Schnack, and J. Killeen, in Ref. 2, p.126

[4] R. A. Clemente and J. L. Milovich, Phys. Lett. A 85, 148 (1981)

[5] J. H. Hammer, Nucl. Fusion 21, 488 (1981)

[6] J. L. Schwarzmeier, D. C. Barnes, D. W. Hewett, C. E. Seyler, A. I. Shestakov, and D. D. Schnack, in Proceedings of the 3rd Symposium of the Physics and Technology of Compact Toroids in the Magnetic Fusion Energy Program (Los Alamos National Laboratory, Los Alamos, NM, 1981)

[7] A. Ishida, H. Momota, and L. C. Steinhauer, Phys. Fluids 31, 3024 (1988)

[8] R. D. Milroy, D. C. Barnes, R. C. Bishop, and R. B. Webster, Phys. Fluids 31, 1224 (1989)

[9] D. C. Barnes, J. L. Schwarzmeier, H. R. Lewis, and C. E. Seyler, Phys. Fluids 29, 2616 (1986)

[10] Z. Mikie and D. C. Barnes, Bull. Am. Phys. Soc. 32, 1728 (1987)

[11] E. J. Horowitz, Ph.D. thesis, University of California, Davis, 1987

[12] M. Tuszewski, D. C. Barnes, R. E. Chrien, J. W. Cobb, D. J. Rej, R. E. Siemon, D. P. Taggart, and B. L Wright, Phys. Rev. Lett. 66, 711 (1991)

[13] D. C. Barnes, R. D. Milroy, Phys. Fluids B. Vol. 3, No. 9, 2609 (1991)

[14] A. V. Gretchikha, J. B. Greenly, D. D. Lee, W. J. Podulka, American Physical Society, 44th Annual Meeting of the Division of Plasma, BP1.048

(2002)

[15] J. B. Greenly, D. A. Hammer, P. D. Pedrow, R. N. Sudan, Phys. Fluids Vol 29, 908 (1986)

[16] W. J. Podulka, D. D. Lee, A. V. Gretchikha, J. B. Greenly, American Physical Society, 46th Annual Meeting of the Division of Plasma Physics, HP1.055 (2004)

[17] H. R. Griem, Plasma spectroscopy, (McGraw-Hill Book Company, New York), (1997)

[18] NRL Plasma Formulary, (Naval Research Laboratory, Washington), 2001

[19] S. C. Brown, Basic Data of Plasma Physics, (The technology press), (1959)